












Research Article

Study on Sintered Wick Heat Pipe (SWHP) with CuO Nanofluids under Different Orientation

P. Manoj Kumar ¹, **Rajasekaran Saminathan** ², **Mohammed Tharwan** ²,
Haitham Hadidi ², **P. Michael Joseph Stalin** ³, **G. Kumaresan** ⁴, **S. Ram** ⁵,
Moti Lal Rinawa ⁶, **P. T. Saravanakumar** ⁷, **K. Karthikeyan** ⁸,
and Dawit Tafesse Gebreyohannes ⁹

¹Department of Mechanical Engineering, KPR Institute of Engineering and Technology, Coimbatore, 641407 Tamil Nadu, India

²Department of Mechanical Engineering, College of Engineering, Jazan University, Saudi Arabia

³Department of Mechanical Engineering, Audisankara College of Engineering & Technology, Gudur, 524101 Andhra Pradesh, India

⁴Department of Mechanical Engineering, Bannari Amman Institute of Technology, Sathyamangalam, 638401 Tamil Nadu, India

⁵Department of Mechanical Engineering, Gokaraju Rangaraju Institute of Engineering and Technology, Hyderabad, 500090 Telangana, India

⁶Department of Mechanical Engineering, Government Engineering College, Jhalawar, Rajasthan 326023, India

⁷Department of Mechatronics Engineering, Hindusthan College of Engineering and Technology, Coimbatore, 641032 Tamil Nadu, India

⁸Department of Mechanical Engineering, Sri Ramakrishna Engineering College, Coimbatore, 641022 Tamil Nadu, India

⁹Department of Mechanical Engineering, Faculty of Manufacturing, Institute of Technology, Hawassa University, Hawassa, Ethiopia

Correspondence should be addressed to Dawit Tafesse Gebreyohannes; dawitt@hu.edu.et

Received 28 March 2022; Revised 4 July 2022; Accepted 8 August 2022; Published 25 August 2022

Academic Editor: Zafar Said

Copyright © 2022 P. Manoj Kumar et al. This is an open access article distributed under the Creative Commons Attribution License, which permits unrestricted use, distribution, and reproduction in any medium, provided the original work is properly cited.

The current work investigates the performance of cylindrical-shaped sintered wick heat pipe at different orientations, numerically. The results are compared and validated with the experimental findings. The study is extended by using a nanofluid (comprising nano-CuO in deionized water) as a working fluid and the thermal performance of heat pipe with deionized (DI) water has been compared with that of heat pipe with nanofluid (containing various concentrations of CuO nanoparticles in DI water). During the investigation, the nanofluid with 1.0 weight fraction of CuO nanoparticles found to be optimum, which has produced the better results. The numerical analysis has been carried out to study the temperature difference, fluid velocity, and pressure drop of the sintered wick heat pipe using the commercial CFD software, Ansys Fluent R14.5. The computational results are observed to be much closer to the experimental data, and the vapor velocity at the heat pipe's core has been determined to be 64.54% higher than the liquid flow over the wick structure. Interestingly, the heat pipe pressure drop has been reduced by adding CuO nanoparticles to the working fluid. Finally, the heat pipe loaded with a 1.0% concentration of nano-CuO in nanofluid has exhibited a notable reduction in pressure drop of 35.33%.

1. Introduction

The nanofluids are the recently developed fluids, which can be considered the sustainable medium of heat transfer appli-

cations. They are also called as the heat transfer fluids for the next generation [1, 2]. The majority of industries are being forced to implement Industry 4.0 to enhance the production rate and to improve the quality of their products. The

equipment used in industries is integrated with the Internet of Things and machine learning technologies [3]. Implementing new ideas will increase plant efficiency; meanwhile, the size and weight of the equipment will also increase. Electronics-based industries are inevitable, which are facing a lot of challenges and undergoing day-by-day changes to compete with the markets in the present and future [4]. The heat pipe works as a superconductor, which has more than 100 times higher thermal conductivity comparing to the copper rod. Owing to their high conductance, these are preferred in lab tops, high-end computers, microprocessors, and solar systems. In IBM computers and workstations, the higher-end processors are producing more heat; the dissipation of the heat from the confined spaces is difficult with conventional sources like blowers. Due to deprived heat removal rate, the CPU's temperature may rise abruptly, which can cause a permanent damage.

The heat management in electronic devices has become complicated because the size reduction and productivity improvement generate high heat flux, which produces mechanical failures in the system or part of the device. Another study [5] analyzed the effectiveness of mesh wick heat pipes filled with CuO nanoparticles based on deionized water. The heat pipe capacity is enhanced by about 31.5% by the delayed dry-out condition. Adham Makki et al. [6] investigated a solar photovoltaic-thermoelectric generator system based on heat pipes. A theoretical model was made, and the performance of the PV cell was improved by putting together PV and TEC parts.

The thermal efficacy of the copper cylindrical heat pipe (HP) using alumina suspended DI water was studied [7]. The efficacy of the HP increased by 16.8% comparing to the base fluid. Yunhua Gan et al. [8] premeditated the heat management of battery packs using cylindrical cell-based heat pipes. A mathematical model had been formed to analyze the distinct achievement of the battery cells and the outcomes had been validated by comparing them with experimental results. They concluded that the upsurge in the length of the heat dissipation section and aluminum sleeves improved the thermal capacity of the system. Wisoot Sanhan et al. [9] experimented with the thermal analysis of the flattened heat pipe with a double heat source to cool the condenser section effectively from the CPU and GPU in laptops. The results indicated that the flat-shaped heat pipe from the circular section reduces the heat resistance by 5.2%. Hassan and Harmand analyzed [10] the effect of a flat-shaped heat pipe which is used to cool the electronic components. A numerical approach was carried out, because the impact of various permeability of the wick structure would be time consuming to attain with the experimental analysis. They revealed that increasing the permeability of the wick structure could lead to a 19.0% drop in heat pipe surface temperature and pressure. Samiya Amir et al. [11] steered a numerical study on solar photovoltaic panels to analyze the capability of heat pipes to remove excessive heat. The incorporation of heat pipes into PV cells attains a temperature reduction of 9°C as compared to the normal panels. Another numerical study [12] was conducted on a U-shaped pulsating heat pipe. The increase in evaporator side temperature shows a uni-directional effect and increases convection as well as boiling heat transfer.

Kumaresan et al. [13] characterized the function of heat pipes by altering the wick structures. They have used sintered, mesh, and sintered-mesh wicks in cylindrical heat pipes. The heat transport capability of the device has increased by about 18.75% as sintered wick structure compared with mesh wicks. Miao et al. [14] identified phase change heat transfer as the best method to transfer high heat flux with minimal losses; a bent copper heat pipe was used in the investigation. The copper-water heat pipe's critical heat flux has been enhanced, and when the working temperature is above 50°C, the increasing slope was obtained. The feasible analysis of sintered copper heat pipes was studied [15] and the notable changes in the distribution of temperature with respect to the axial distance in the heat pipe, and characteristics limits are evaluated. When the bend angle of the copper heat pipe is raised, the thermal efficacy of the HP is seen to be lowered. Jing et al. [16] explored the capacity and transport limitations of the HP by varying the wick structure's permeability. The capillary limitation is measured in the way of accounting for the capillary pressure, porosity, and permeability of the heat pipe. The results proved that the irregular powder surface of the sintered wick structure reduces 30% of the capillary pressure compared with spherical-shaped powders.

A study was conducted on the heat pipe porous wick structure by Hui Li et al. [17]. The authors confirmed that the capillary limitation of the heat pipe is directly influenced because of the particle size of the powder used to prepare the wick structure. Jafari et al. [18] analyzed the thermal characteristics of additively manufactured wick for heat pipes. The wick structure is manufactured with a multi-scale sintered powder that improves the properties of the wick structure. The flat heat pipe's thermal efficacy had been improved, when it was occupied with 110% of working fluid. Vijayakumar et al. [19] used CuO and alumina nanoparticles in the sintered wick HP to improve the convection heat transmission properties and permeability of the HP. The author found the optimum concentration achieved for CuO nanoparticles at 1.0 wt%. The optimum results were obtained for both CuO- and alumina-based heat pipes at a 45° inclination angle. The thermal characteristics at the evaporator as well as condenser regions had been increased to 32.90% and 24.51%, respectively, at the optimum tilt angle. Brautsch and Kew [20] used different kinds of mesh wicks in the HP. The outcomes confirmed the number of layers wounded in the tube could develop the heat pipe's effectiveness.

As of now, the literature does not justify the impact of porosity and permeability of the wick structure on the thermal performance enhancement of the HP. Ich-Long Ngo and Chan Byon [21] numerically investigated the performance of sintered wick heat pipes measuring their porosity and permeability. They proved that the permeability of microporous inverse wicks produces high performance depending on the wick configuration and porosity. Shiwei Zhang et al. [22] analyzed the capillarity characteristics of sintered powder-based wicks in stainless steel heat pipes. The authors experimentally measured the permeability and porosity of irregular- and regular-sized particles. The irregular-sized particles had proved a better permeability in

terms of 1.5–4.8 factors. The hybrid nanofluids are another variety of heat transfer mediums with a wide range of uses, including electronic cooling, IC engine cooling, heat pipes, and heat exchangers, coolants in welding and machining, nuclear facilities, and many more. Bumataria et al. [23] premeditated the use of heat pipes with the presence of different nanoparticle combinations with the base fluids. The nanofluids containing CuO as well as ZnO nanoparticles and their hybrid mixture in 25:75, 50:50, and 25:75 mass ratios had been chosen by Bumataria et al. [24] while preparing aqueous nanofluids with 1.0 wt. percent of aforementioned nanoparticle combinations. In a copper heat pipe with a straight tube shape, a two-phase heat transfer study had been accomplished using 60% of the evaporator volume to fill the working fluid. The heat input was adjusted from 60 W to 160 W, and the tilt was accustomed from 0° to 90° in 15° and 20 W steps. The hybrid nanofluid comprising nanoparticles of CuO and ZnO (75:25) in water demonstrated the least increase in thermal resistance compared to base fluid. The authors speculated that individual nanostructures in the base medium might have induced a synergistic impact, which would have demonstrated the hybrid's improved behavior. At 60° inclination angle and a 160 W heat input, the nanofluids have performed in a better manner comparing to other tilt angles and heat inputs. A cylinder-shaped heat pipe with a copper screen mesh type of wick structure was explored by another literature [25] and its construction was improved by utilizing the investigational data for nanofluids. The base fluid had been mixed with Al₂O₃, CuO, and ZnO nanoparticles at a concentration of 1.0 wt percent. The experimental results were compared, particularly in terms of heat load (in a range of 60–160 W with 20 W incremental steps) and inclination angle (in a range of 0° to 90° with 15° incremental steps). The results ascertained that the nanofluids with CuO nanoparticles displayed a better thermal enhancement comparing to other working fluid at the inclination of 60°.

The extensive review on the published literature revealed that the incorporation of sintered wicks with regular-sized particles could increase strength and durability of the wicks; however, the effect of such particles on the permeability characteristics and performance of the HP wick had not been properly dealt. The use of sintered wick in heat pipes proved to have the greatest influence on the capillary action of the working medium. The novelty of the present work is that it has proposed and experimented the application of irregular-sized copper particles to produce non-uniform pores in the sintered wick structure for enhancing the permeability as well as performance of the heat pipe, which was not adequately addressed in the literature. The numerical analysis of the sintered wick heat pipe has also been performed and the obtained results are validated by comparing them with the experimental results. Further, the investigation has been extended with the aid of nanofluid containing different weight fraction of nano-CuO particles within the heat pipe as working medium and the optimum operating condition and orientation angle are explored.

2. Properties of CuO nanofluid

The CuO nanoparticle (97.5% pure) is a commercial product of Alfa Aesar, USA. However, CuO nanoparticles are allowed for a high-energy ball milling process, which is operated at a 1200 rpm speed to uniform its size. The ball to particle ratio is chosen as 5.21 and the process is extended to a 12-hour period. After the process, the size of nanoparticles is confirmed using HRTEM characterization. Thereafter, the crushed copper (II) oxide nanoparticles are suspended in 250 ml of DI water and taken in a flask. The ultrasonicated (duration of one hour) solution is brought into the stability analysis. This fluid is kept statically for two months. During this period of time, no particles settle, and it confirms that the prepared solution is stable.

The dimension and morphology of the nanoparticles show a major impact on the thermophysical properties of prepared nanofluids [26]. The particles that are larger than 100 nm could be easily settled in the prepared solution, and irregular-shaped nanoparticles may affect the fluid flow properties [27]. Figure 1 reports the HRTEM of nano-CuO particles used in this study. The report confirms the size of the nanoparticles is around 40 nm and fully spherical-shaped nanoparticles are suspended in the fluid to improve the Brownian motion and viscosity of the nanofluid. Figure 1 attests to the size and shape of CuO nanoparticles used in this study.

3. Experimental Facility

The experimental test facility is created using calibrated instruments and the layout setup given in Figure 2. Copper element is selected as pipe wall material, sintered wick powder, and nanoparticles in this study because it is having highest thermal conductivity value in the metal segment, as well as flexible for fabrication. The outer surface and inner core temperature, volume flow rate of cooling water supplied for the condensation process, and heat distributed to the ceramic heater are measured. The heat pipe test section is coupled with ten T-type thermocouples. Five of each thermocouple are fixed at the outer surface and inner core of the HP. A refrigerant-based temperature control unit is attached to the experimentation, used to remain the cooling water entry temperature to the condenser section. An AC power variac controls the electric power supply to the ceramic heater, which confirms the correct heat input at the primary part of the HP. A digital logger is used to examine the steady-state values from the investigations. The experimentation was conducted under atmospheric conditions, i.e., 1 bar pressure and a 27°C temperature. The observations are made at steady-state conditions. Approximately 45 minutes duration is maintained between each measurement.

4. Uncertainty Results

The uncertainty involved in the experimental work is evaluated based on Holman [28]. The surface temperature and mass flow rate of cooling water are the derivatives measured during the experimentation. The uncertainty of experimental values has been determined and given in Table 1.

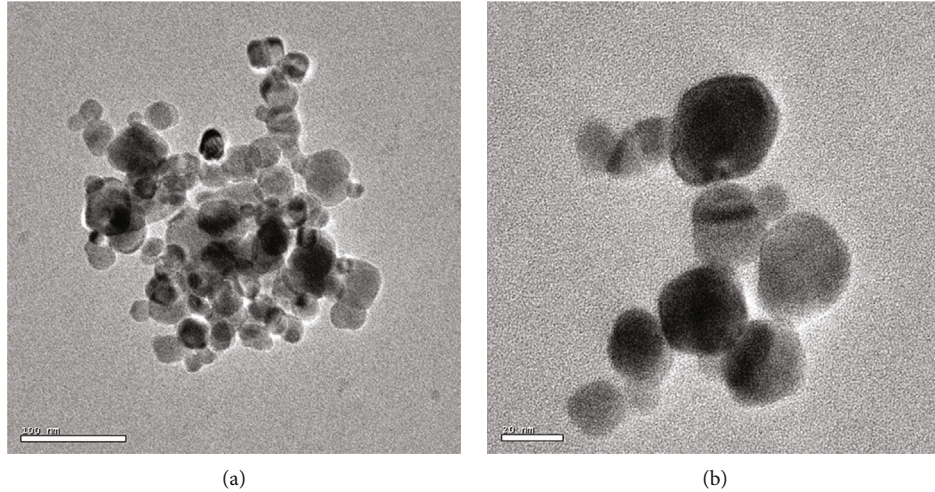


FIGURE 1: High-resolution TEM images of CuO nanoparticles with (a) 100 nm and (b) 20 nm magnification.

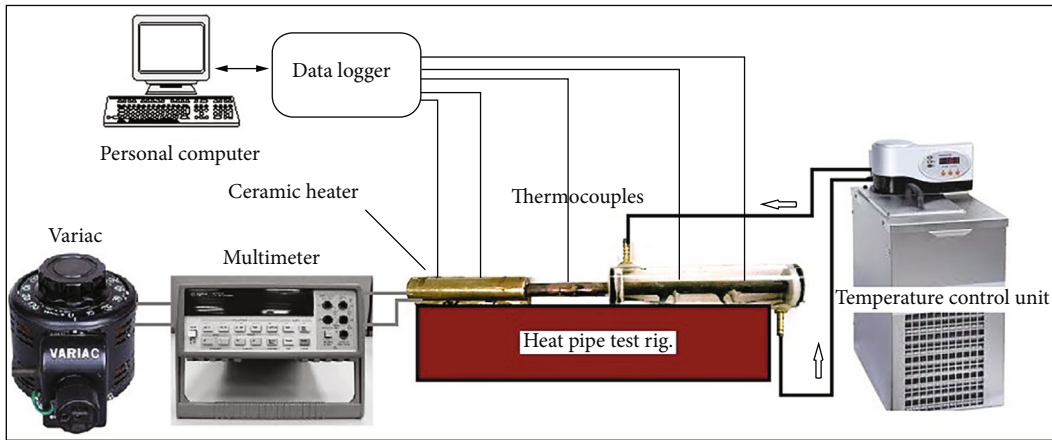


FIGURE 2: Schematic layout of experimental test rig.

TABLE 1: Uncertainty of the quantities.

| S. No | Quantity | Uncertainty (%) |
|-------|------------------------|-----------------|
| 1. | Heat input | 0.329 |
| 2. | Temperature difference | 0.12 |
| 3. | Thermal resistance | 1.716 |

5. Numerical Procedure

Experimental investigations of engineering problems are essential in order to know the physical phenomena of the problem. Moreover, solution accuracy and reliability are also high in the experimental study. However, it has a few limitations, such as high cost, more time, equipment cost, and maintaining steady-state conditions and operating parameters. Under these circumstances, numerical analysis comes in handy [11]. In this study, a two-dimensional numerical analysis was performed using the commercial CFD software ANSYS FLUENT R 14.5. The CFD results were verified by the experimental results. Further, the application of CFD is

rapidly expanding with the growth in computational resources. The verification is helpful in identifying and quantifying the errors in modeling and the solution. The accuracy of the numerical analysis is affected by the assumptions made in the boundary conditions applied and the errors like discretization, truncation, and rounding off. In the current investigation, a numerical approach was performed for the copper sintered HP to easily tackle the design complications of two-phase heat transfer, liquid state fluid flow through the wick structure, the interface between the gaseous, and liquid regions.

The geometrical dimensions of the HP used in the experimental investigations are shown in Table 2. A chemically cleaned copper pipe was selected to fabricate the HP with the outer section and a copper powder-based sintered wick with a 1 mm thickness is the wick structure of the heat pipe. Sintered wick with a thickness and porosity of 1 mm and 0.48, respectively, are considered. Because of symmetry about the axis, only half of the section was taken in the analysis. In this work, the grid dependence test was conducted in

TABLE 2: Specifications of sintered wick heat pipe.

| Sl. No | Description | Value |
|--------|---------------------------|---------------|
| 1. | Heat pipe material | Copper |
| 2. | Total length | 330 mm |
| 3. | Evaporator length | 100 mm |
| 4. | A diabatic length | 80 mm |
| 5. | Condenser length | 150 mm |
| 6. | Outer diameter | 12 mm |
| 7. | Wick material | Copper |
| 8. | Wick thickness | 1 mm |
| 9. | Wick type | Sintered wick |
| 10. | Quantity of working fluid | 7.3 ml |
| 11. | Working pressure | 13.45 kPa |

order to ensure the optimized number of grids and size. For this test, the heat pipe's surface temperature was measured. Its values were compared to three different grid sizes and a grid size of 112 x 86 gave a surface temperature value closer to the experimental value and was taken as the optimum.

6. Boundary Conditions

The following assumptions were made in the numerical analysis of the heat pipe [12].

- (i) Laminar and incompressible liquid flows
- (ii) At $t=0$ (time), the vapor was saturated
- (iii) All of the thermophysical properties of CuO nanofluid/DI water are assumed to stay the same throughout the experiment, except for the vapor flow density, which is calculated based on the pressure at a certain point
- (iv) Except for the evaporator and condenser units, the entire heat pipe region has been insulated
- (v) The heat pipe saturation temperature was estimated at each location depending on the local pressure

The working fluid, i.e. 1.0% weight concentration of CuO nanofluid/deionized water, is considered in the surface area of the wick structure and the gaseous state in the central core area of the HP. When heat is given in the evaporator region, the CuO nanofluid/DI water gets vaporized and is converted to a gaseous state, and the vapor travels to the condenser region. The vapor reaches the cooling side at the opposite end of the HP. It follows the wick surfaces back to the starting point of the heat pipe.

7. Governing Equations

The fundamental principles governing liquid/vapor flow and heat density variation are mathematically formulated using the PDE (partial differential equation) equation. When the Reynolds number for the vapor flow was in the range of 50 to 500, the laminar flow was taken. Also, when the temper-

ature varies with time at a point, the problem is called unsteady.

7.1. Vapor Flow Region. Continuity equation:

$$\frac{\partial \rho_v}{\partial t} + \frac{1}{r} \frac{\partial}{\partial r} (\rho_v r V_v) + \frac{\partial}{\partial z} (\rho_v W_v) = 0. \quad (1)$$

Momentum equation:
R-momentum

$$\begin{aligned} \rho_v \left[\frac{\partial V_v}{\partial t} + V_v \frac{\partial V_v}{\partial r} + W_v \frac{\partial V_v}{\partial z} \right] \\ = - \frac{\partial p_v}{\partial r} + \mu_v \left[\frac{\partial^2 V_v}{\partial z^2} + \frac{4}{3r} \frac{\partial}{\partial r} \left(r \frac{\partial V_v}{\partial r} \right) + \frac{1}{3} \frac{\partial^2 W_v}{\partial z \partial r} - \frac{4}{3} \frac{V_v}{r^2} \right]. \end{aligned} \quad (2)$$

Z-momentum

$$\begin{aligned} \rho_v \left[\frac{\partial W_v}{\partial t} + V_v \frac{\partial W_v}{\partial r} + W_v \frac{\partial W_v}{\partial z} \right] = - \frac{\partial p_v}{\partial z} \\ + \mu_v \left[\frac{4}{3} \frac{\partial^2 W_v}{\partial z^2} + \frac{1}{r} \frac{\partial}{\partial r} \left(r \frac{\partial W_v}{\partial r} \right) + \frac{1}{r} \frac{\partial}{\partial r} \left(r \frac{\partial V_v}{\partial z} \right) - \frac{2}{3} \frac{\partial}{\partial z} \left[\frac{1}{r} \frac{\partial}{\partial r} (r V_v) \right] \right]. \end{aligned} \quad (3)$$

Energy equation

$$\begin{aligned} \rho_v C_{pv} \left[\frac{\partial T_v}{\partial t} + V_v \frac{\partial T_v}{\partial r} + W_v \frac{\partial T_v}{\partial z} \right] = k_v \frac{1}{r} \frac{\partial}{\partial r} \left(r \frac{\partial T_v}{\partial r} \right) \\ + \frac{\partial^2 T_v}{\partial z^2} + V_v \frac{\partial p}{\partial r} + W_v \frac{\partial p}{\partial z} + \mu_v \varphi, \end{aligned} \quad (4)$$

where φ = dissipation rate, given by

$$\begin{aligned} \varphi = Z \left[\frac{\partial V_v}{\partial r} + \left(\frac{V_v}{r} \right)^2 + \left(\frac{\partial W_v}{\partial z} \right)^2 \right] + \left[\frac{\partial V_v}{\partial z} + \left(\frac{\partial W_v}{\partial r} \right)^2 \right] \\ - \frac{2}{3} \left[\frac{1}{r} \frac{\partial}{\partial r} (r V_v) + \left(\frac{\partial W_v}{\partial r} \right)^2 \right]. \end{aligned} \quad (5)$$

7.2. CuO Nanofluid/DI Water Region. The working fluid passes by capillary action and is primarily influenced by the flow through a porous material. Porosity and permeability are the important parameters that decide the capillary function of the wick structure. The experimentally measured values of the copper sintered wick structure were used in this analysis [29]. The CuO nanofluid/DI water flow is assumed as an incompressible medium. The viscosity between the layers is high (laminar) and unsteady flow conditions.

Continuity equation:

$$\frac{1}{r} \frac{\partial}{\partial r} (r V_l) + \frac{\partial W_l}{\partial z} = 0. \quad (6)$$

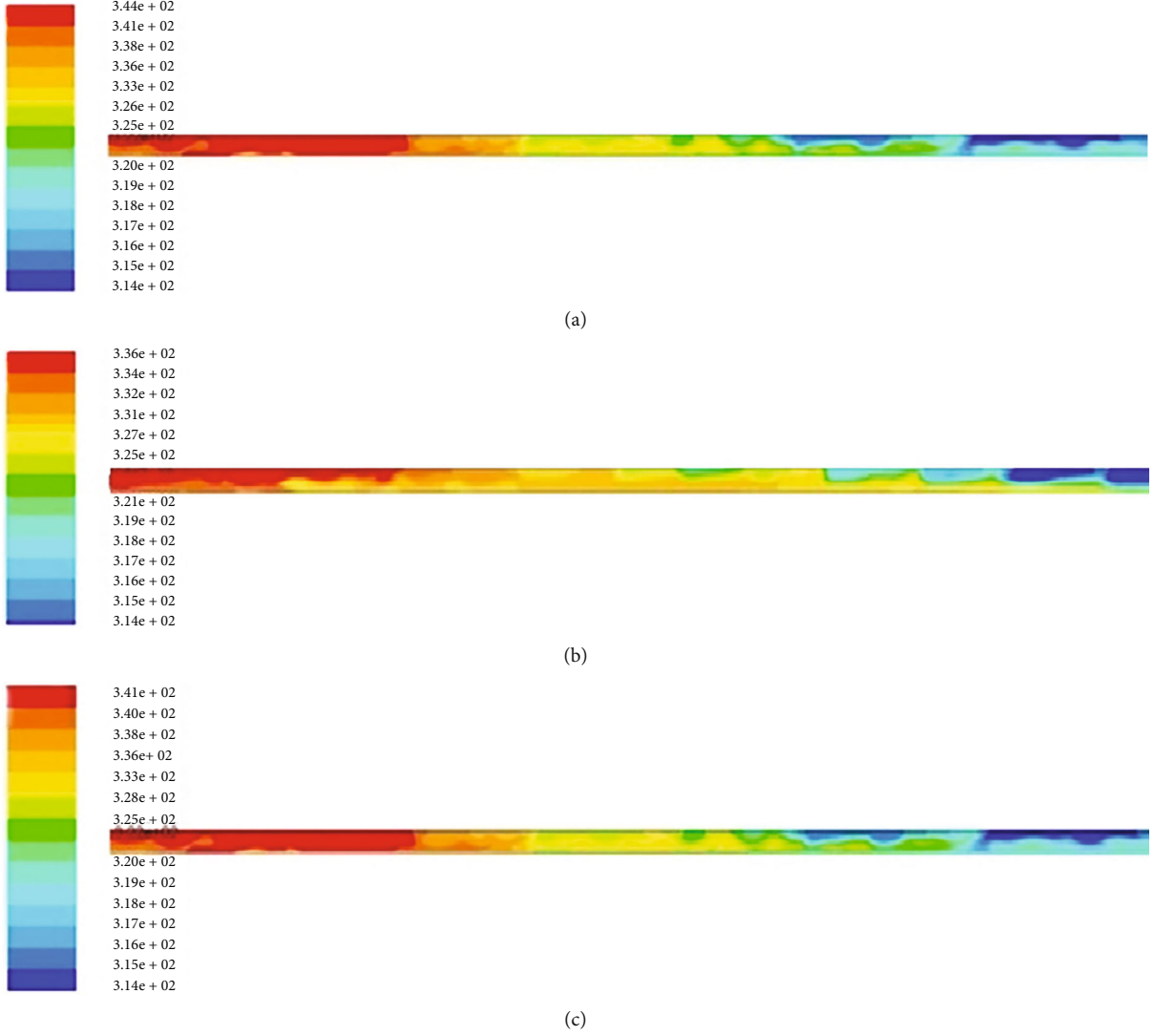


FIGURE 3: Surface temperature distribution (in Kelvin) over the length of heat pipe with DI water for various tilt angles: (a) 0°, (b) 45°, and (c) 90°.

R-momentum

$$\frac{1}{\varepsilon} \left[\frac{\partial V_l}{\partial t} + \frac{1}{\varepsilon} \left(V_l \frac{\partial V_l}{\partial r} + W_l \frac{\partial V_l}{\partial z} \right) \right] = -\frac{1}{P_l} \frac{\partial P_l}{\partial r} - \frac{\mu_l V_l}{P_l k_l} + \frac{\mu_l}{P_l \varepsilon} \left[\frac{\partial^2 V_l}{\partial z^2} + \frac{1}{r} \frac{\partial}{\partial r} \left(r \frac{\partial V_l}{\partial r} \right) - \frac{V_l}{r^2} \right], \quad (7)$$

where ε is the wick porosity.

Z-momentum

$$\frac{1}{\varepsilon} \left[\frac{\partial W_l}{\partial t} + \frac{1}{\varepsilon} \left(V_l \frac{\partial W_l}{\partial r} + W_l \frac{\partial W_l}{\partial z} \right) \right] = -\frac{1}{P_l} \frac{\partial P_l}{\partial z} - \frac{\mu_l W_l}{P_l k_l} + \frac{\mu_l}{P_l \varepsilon} \left[\frac{\partial^2 W_l}{\partial z^2} + \frac{1}{r} \frac{\partial}{\partial r} \left(r \frac{\partial W_l}{\partial r} \right) \right]. \quad (8)$$

Energy equation

$$\rho_l C_{pl} \left[\frac{\partial T_l}{\partial t} + V_l \frac{\partial T_l}{\partial r} + W_l \frac{\partial T_l}{\partial z} \right] = \frac{1}{r} \frac{\partial}{\partial r} \left(r k_{\text{eff}} \frac{\partial T_l}{\partial r} \right) + \frac{\partial}{\partial z} \left(k_{\text{eff}} \frac{\partial T_l}{\partial z} \right), \quad (9)$$

where, the effective thermal conductivity, k_{eff} is given by

$$K_{\text{eff}} = \frac{K_l [(K_l + K_s) - (1 - \varepsilon)(K_l - K_s)]}{(K_l + K_s) + (1 - \varepsilon)(K_l - K_s)}. \quad (10)$$

7.3. Heat Pipe Wall Region.

$$\rho_w C_{pw} \frac{\partial T_w}{\partial t} = k_w \left[\frac{1}{r} \frac{\partial}{\partial r} \left(r \frac{\partial T_w}{\partial r} \right) + \frac{\partial^2 T_w}{\partial z^2} \right]. \quad (11)$$

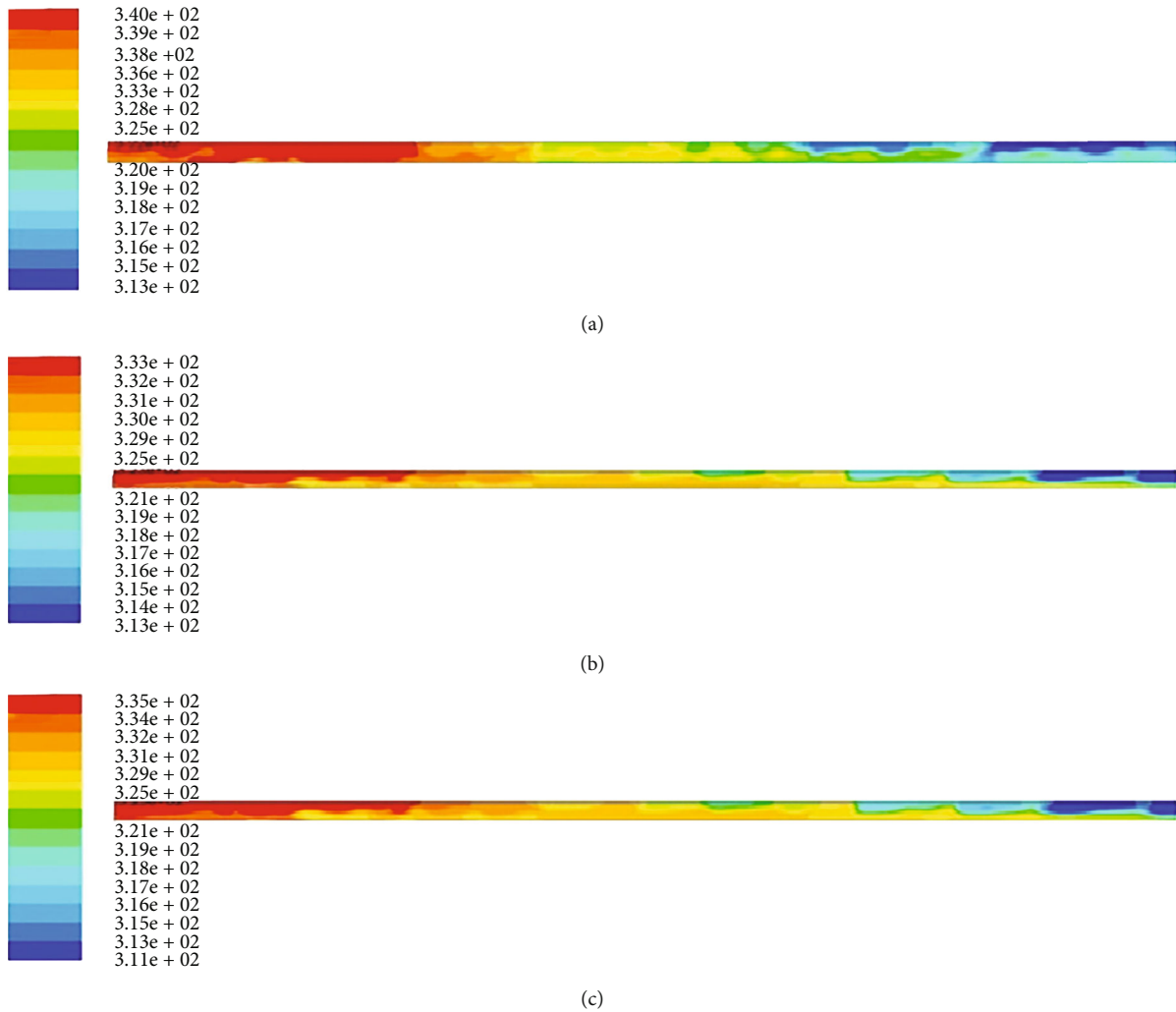


FIGURE 4: Surface temperature distribution (in Kelvin) over the length of the heat pipe with 1.0 wt.% of CuO/DI water nanofluid for various tilt angles: (a) 0°, (b) 45°, and (c) 90°.

8. Results and Discussion

A numerical analysis has been carried out to study the temperature difference, fluid velocity, and pressure reduction in the sintered wick HP using the commercial CFD software Ansys Fluent R14.5. The surface and vapor core temperatures of the SWHP are continuously monitored using a personnel computer followed by a high-accuracy data acquisition system. After that, numerical results are validated by comparing them with experimental values.

8.1. Temperature Distribution. The outer side temperature for SWHP with deionized water and a 1.0% weight concentration of CuO-based nanofluid is seen in Figures 3(a)–3(c) and 4(a)–4(c). In these conditions, 300 K and 13.45 kPa are considered to represent the starting temperatures and pressures, respectively. All the temperature contours are plotted at 100 W of heat input. The analysis was conducted for the varying tilt angles of 0, 45, and 90°. The outside temperature

of the heating region is drastically higher than the vapor passage temperature. The temperature difference between the evaporator and condenser regions is approximately 30°C, as observed for deionized water heat pipes in a parallel orientation. The distribution of temperature decreased during the tilted condition of HP, because of the lower thermal resistance at the tilted position.

The surface temperature is considerably decreased when the HP has been angled to a 45°. The temperature distribution follows the same trend as that of the horizontal position, but a significant decrease has been noticed. This is because the leaning of the HP increases the capillary function, which makes the return of the condensate to the evaporator section easy. However, the performance deteriorates once the heat pipe has been tilted to 90°. For 0°, 45°, and 90°, the thermal gradient between the heating and cooling region is 30°C, 23°C, and 27°C, respectively. The larger inclination angle helps to enhance rate of return of working fluid from the cooling region.

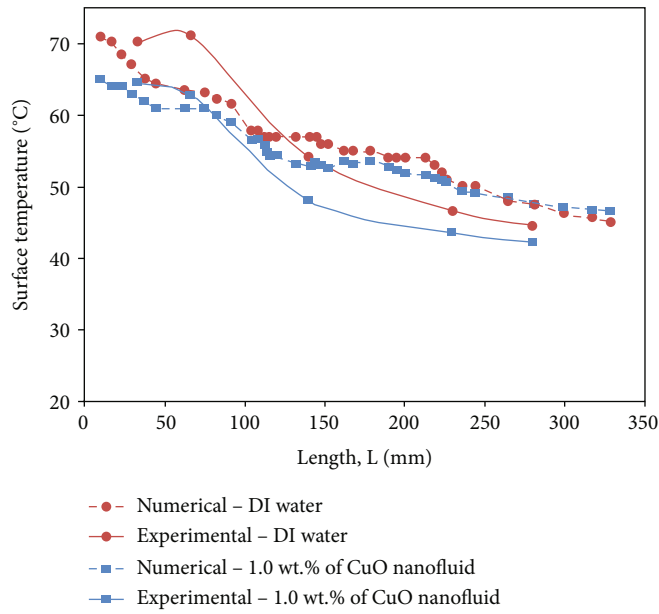


FIGURE 5: Surface temperature distributions (in Kelvin) along its length for a tilt angle of 45°.

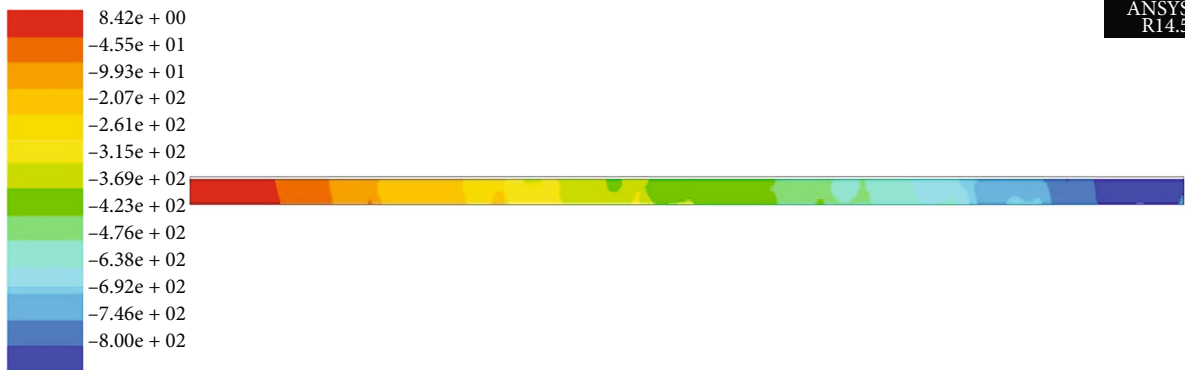


FIGURE 6: Pressure contour (in Pa) of the heat pipe along with its axial length for DI water.

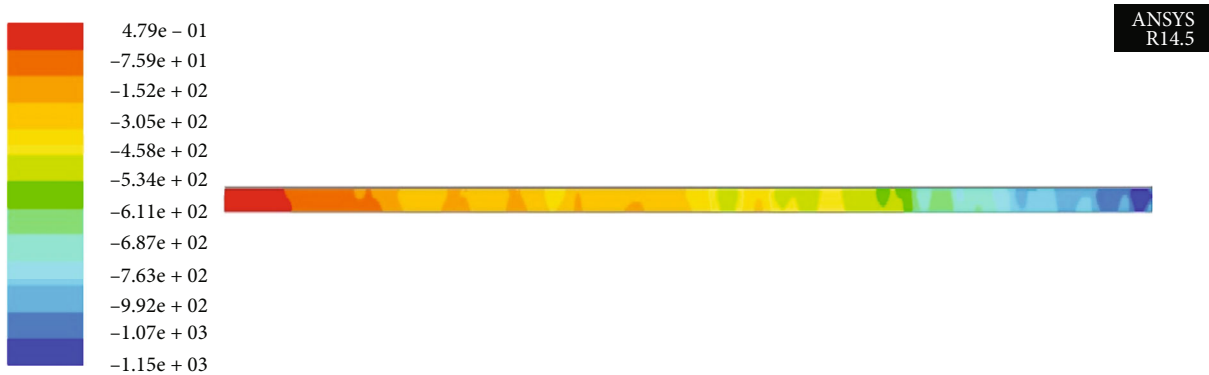


FIGURE 7: Pressure contour of the heat pipe along its axial length for CuO nanofluid with 1.0 wt.%.

The liquid film formation at the condenser part may also affect the heat removal rate. Hence, the surface temperature increases for the heat pipe at the vertical position.

The spherical-shaped, 40 nm (preferably small in size) CuO nanoparticles improved the thermal as well as fluid flow properties of the working medium. The heat-

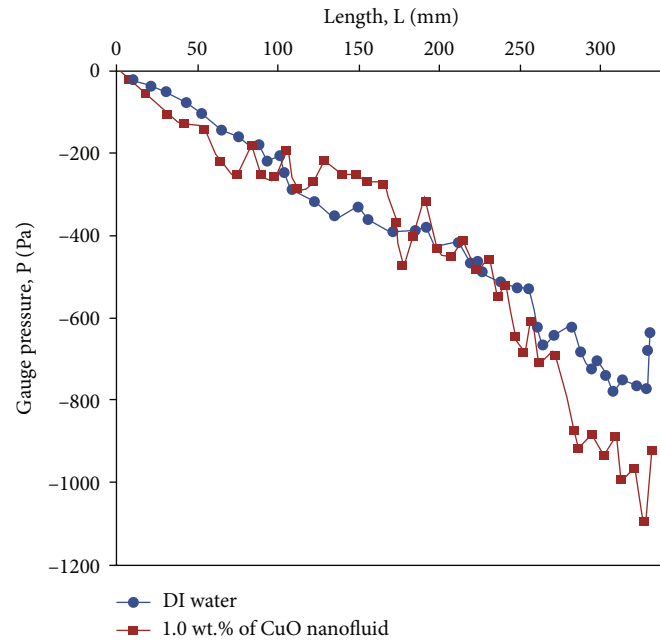


FIGURE 8: Comparison of vapor pressure of heat pipe working without and with CuO nanofluid for 45° orientation angle.

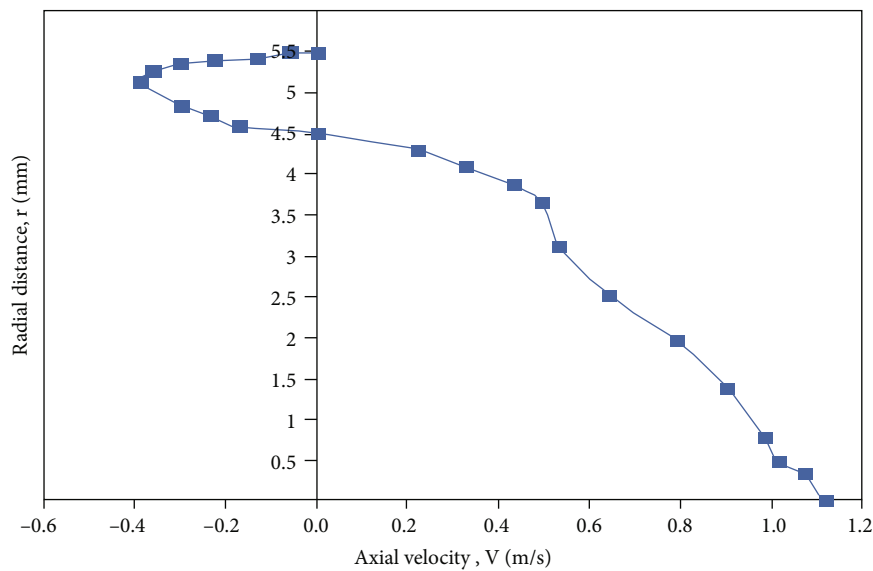


FIGURE 9: Axial velocity distribution at a diabatic section ($X=135$ mm from evaporator end) in radial direction of the heat pipe with nanofluid concentration 1% at tilt angle of 45°.

absorbing capacity of the base fluid will be increased by adding uniform-sized nanoparticles. Moreover, the liquid-vapor interface is properly steam lined and thus also shows enhancement in the results. The observed T values are 27, 20, and 24°C, respectively, which are considerably lower as compared to the DI water results.

Figure 5 depicts the heat pipe's surface temperature distribution obtained from experimental and numerical studies at 100 W of heat input. In the experimental analysis, thermocouples are located at fixed intervals, with the last thermocouple at a distance of 50 mm from the con-

denser, whereas in the numerical analysis, the full length of the heat pipe is considered. Moreover, the inclusion of copper (II) oxide nanoparticles results in the surface temperature reduction of the HP. The minimum and maximum deviations in the temperature distributions for the numerical and experimental values are 4.77% and 13.64%, respectively. This difference is greatest in the condenser section, because of the uncertainties associated with condenser cooling. The temperature difference is the dominant parameter in the present work. The main objective of the study is to enhance the capacity of the heat pipe

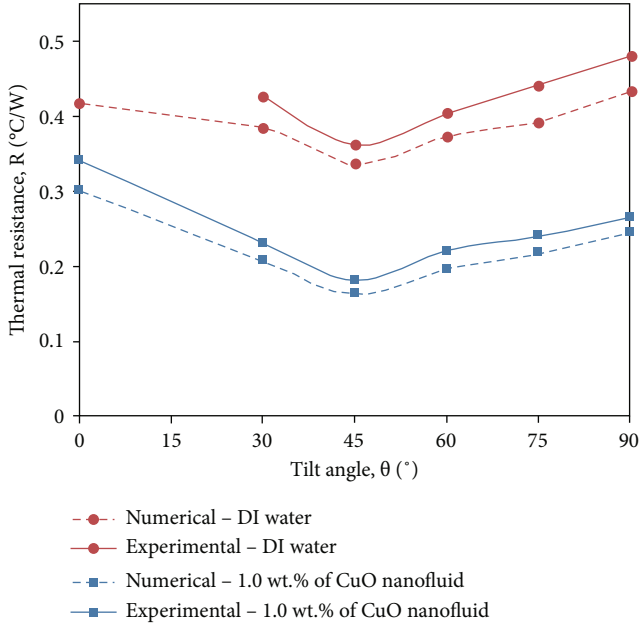


FIGURE 10: Effect of orientation angle on the thermal resistance of deionized water and CuO nanofluid heat pipe (input=120 W) compared with Kumaresan et al. [30].

by changing the orientation as well as functioning conditions. The operation of the heat pipe is absolutely dependent on the dry-out condition. It may be postponed by lowering the temperature between the evaporator and condenser section. So, the difference between the surface temperature and the vapor temperature is the most important factor in how well heat pipes work.

8.2. Pressure Distribution. The pressure distribution of the SWHP for DI water and CuO-based working fluid with a 1.0% weight concentration is presented in Figures 6 and 7. The temperature, pressure, and velocity distribution in a heat pipe are calculated using the mass, momentum, and energy equations. At each point, the pressure value varies because of the temperature and phase changes. In the evaporator region, the pressure is at its maximum because of its higher temperature. The vapor core pressure gradually decreases over the length of the condenser.

The local pressure has a direct effect on the saturation temperature of the liquid, which is given by the equation,

$$T_0 = \left[\frac{1}{T_o} - \frac{R}{h_{fg}} \cdot \ln \frac{P_s}{P_o} \right], \quad (12)$$

where P_o and T_o are the saturation pressure and temperature, respectively, and P_s is the vapor pressure.

In addition, it is observed that due to the inclusion of the CuO nanoparticles, the local pressure deteriorated due to the reduction in temperature at all the locations. The suspension of CuO nanoparticles suppressed the thermal resistance and thus the capillary action of the liquid from the condenser section is increased. It results in a drop in vapor core and surface temperature. The pressure gets proportionally

reduced with respect to the temperature as per Charles's law. It is also perceived that the pressure drop in the case of a nanofluid is more than the base fluid as the suspended CuO particles raise the viscosity and give rise to more pressure drop. Figure 8 illustrates the gauge pressure of the heat pipe with respect to the axial length. The pressure distribution curve is formed in the negative direction because the heat pipe is working under vacuum pressure. The pressure is evenly distributed for DI water heat pipe comparing to the CuO nanofluid. The heat pipe using CuO nanofluid, on the other hand, achieves the lowest pressure.

8.3. Axial Velocity Distribution. The axial velocity variation of the SWHP in the radial direction is plotted in Figure 9. The readings are taken from the adiabatic section of the HP. The axial velocity of the vapor flow is extremely high at the center core of the heat pipe and zero at the surface region due to the no-slip conditions. After that, the graph passes in the negative direction, because the working fluid is flowing in the reverse direction. The maximum velocity of vapor flow is 1.1 m/s whereas it is only 0.39 m/s for liquid flow, which clearly shows the vapor velocity is more than double the time of that of nanofluid/DI water flow in the vapor core region.

8.4. Result Validation. The SWHP heat resistance is estimated experimentally using the temperature differential between the heating and cooling regions. The heat delivered to the heating end is estimated from the current and voltage values noted from the data logger. It can be found in [19].

$$R_{hp} = \frac{\Delta T_s}{Q_{in}}, \quad (13)$$

where $\Delta T_s = \bar{T}_e - \bar{T}_c$.

Figure 10 represents the heat resistance of SWHP for the cases of CuO nanofluid and DI water at a 120 W heat supply. The heat resistance reduces with the upsurge tilt angle till 45° but tends to rise for inclination angles greater than that. At a 45° inclination angle, 1.0 wt.% CuO/DI water nanofluid shows a maximum decrease of 49.46% when compared to DI water. The experimental results of the horizontal DI water heat pipe are not represented in the graph. This is due to the attainment of dry-out at this angle. The results obtained from the numerical study show lower thermal resistance than the experimental value, and this may be due to the approximation made in the numerical analysis. A maximum of 13.06% deviation is observed between the studies for heat pipes filled with deionized water.

The heat flux of the heat pipe is compared with [29] for the optimal weight concentration of 1.0% of CuO-based working fluid. The tilt angle of the heat pipe increases from a flat to a perpendicular position. The numerical findings match well with the experimental results. The thermal resistance is high irrespective of the working fluid when the HP is operating in a horizontal position. Thermal resistance attained its lowest value at an ideal tilt angle of 45°. Numerical values registered the lowest thermal resistance value compared with experiments. This is because the data prediction is more accurate in numerical, whereas the experimental uncertainties influence the

experimental values. The greatest drop in heat resistance is $0.181^{\circ}\text{C}/\text{W}$ for numerical prediction, which is 5.78% lower than the experimental values. Zafar Said et al. [31] and Stalin et al. [32] confirmed that the introduction of high conductive nanoparticles within the working medium could enhance the heat transfer properties at a determined optimum weight fraction.

9. Conclusion

The numerical analysis of the irregular-shaped copper particles imposed sintered wick heat pipe was conducted using CuO nanofluids as working fluid, and the findings were validated by comparing them with the experimental data. The following observations are made after critical analysis:

- (i) A strong consensus was observed between the numerical and experimental investigations. The minimum and maximum deviations in surface temperature had found to be 4.77% and 13.64%, respectively
- (ii) The pressure at the evaporator section was at its maximum, and it had been gradually reduced, while moving towards the condenser section. When 1.0% weight fraction of CuO nanoparticles was supplemented, the heat pipe's vapor pressure had gone down compared to heat pipe with plain DI water
- (iii) The pressure drop, which occurred in the heat pipe using CuO nanofluids, was greater compared with the plain DI water, because of the restriction to fluid flow created by the nanofluid
- (iv) With a weight concentration of 1.0% nano-CuO in nanofluid, the pressure drop in heat pipe had been decremented by 35.33%.
- (v) The axial velocity of the vapor core was high at the heat pipe's central core and zero velocity was found near the surface of the sintered wick structure. The vapor velocity at the heat pipe's core was 64.54% higher than the liquid flow over the wick structure. Axial vapor flow velocity was found to be 2.8 times greater than the liquid phase
- (vi) The thermal resistance of the heat pipe was reduced by 49.46%, when 1.0% CuO nanoparticles had been used. Contrarily, the required values had not been obtained, when the heat pipe was being operated in a horizontal orientation due to its dry-out condition. However, the data was predicted during the numerical analysis

Nomenclature

A: Area (m^2)
 d: Particle size (nm), thickness of heat pipe
 g: Body force/gravity
 I: Current
 k: Effective thermal conductivity ($\text{W}/\text{m}^{\circ}\text{C}$)
 m: Mass (kg)

P: Pressure (N/m^2)
 r: Radius (mm)
 T: Temperature ($^{\circ}\text{C}$)
 V: Voltage (Volts), velocity (m/s)
 W: Axial flow velocity (m/s)
 ΔT : Difference in temperature ($^{\circ}\text{C}$).

Subscript

bf: CuO nanofluid/DI water
 c: Cooling end/condenser
 e: Heating end/evaporator
 eff: Effective
 fg: Phase change
 hp: Heat pipe
 max: Maximum
 ph: Phase transition
 Q: Power input
 q: Heat density
 r: Radial coordinate
 th: Thermal
 v: Vapor
 w: Wick.

Greek Symbols

θ : Orientation of heat pipe (degree)
 ε : Wick porosity
 μ : Dynamic viscosity (Ns/m^2)
 ρ : Density (kg/m^3)
 φ : Volume fraction (%)
 ω : Weight concentration (wt.%)
 Δ : Increment/decrement.

Data Availability

The data used to support the findings of this study are included within the article.

Conflicts of Interest

The authors declare that there is no conflict of interest regarding the publication of this paper.

References

- [1] P. M. J. Stalin, T. V. Arjunan, M. M. Matheswaran, and N. Sadanandam, "Effects of CeO_2 /water nanofluid on the efficiency of flat plate solar collector," *Journal of the Chinese Society of Mechanical Engineers*, vol. 41, pp. 75–83, 2020.
- [2] M. Vijayakumar, S. Sivankalai, P. Michael Joseph Stalin, G. Kumaresan, P. Selvakumar, and V. Manikandan, "A scientific analysis on development of nanofluids for heat transfer and fluid flow applications," *Solid State Technology*, vol. 64, pp. 3667–3684, 2021.
- [3] V. Alcácer and V. Cruz-Machado, "Scanning the Industry 4.0: a literature review on technologies for manufacturing systems," *Engineering Science and Technology, an International Journal*, vol. 22, no. 3, pp. 899–919, 2019.
- [4] P. M. Kumar, R. Saminathan, A. Sumayli et al., "Experimental analysis of a heat sink for electronic chipset cooling using a

- nano improved PCM (NIPCM),” *Materials Today: Proceedings*, vol. 56, pp. 1527–1531, 2022.
- [5] G. Kumaresan, S. Venkatachalapathy, and I. C. Naik, “An experimental study on improvement in thermal efficiency of mesh wick heat pipe,” *Applied Mechanics and Materials*, vol. 592-594, pp. 1423–1427, 2014.
 - [6] A. Makki, S. Omer, Y. Su, and H. Sabir, “Numerical investigation of heat pipe-based photovoltaic–thermoelectric generator (HP-PV/TEG) hybrid system,” *Energy Conversion and Management*, vol. 112, pp. 274–287, 2016.
 - [7] T.-P. Teng, H.-G. Hsu, H.-E. Mo, and C.-C. Chen, “Thermal efficiency of heat pipe with alumina nanofluid,” *Journal of Alloys and Compounds*, vol. 504, Supplement 1, pp. S380–S384, 2010.
 - [8] Y. Gan, L. He, J. Liang, M. Tan, T. Xiong, and Y. Li, “A numerical study on the performance of a thermal management system for a battery pack with cylindrical cells based on heat pipes,” *Applied Thermal Engineering*, vol. 179, article 115740, 2020.
 - [9] W. Sanhan, K. Vafai, N. Kammuang-Lue, P. Terdtoon, and P. Sakulchangsattajai, “Numerical simulation of flattened heat pipe with double heat sources for CPU and GPU cooling application in laptop computers,” *Journal of Computational Design and Engineering*, vol. 8, no. 2, pp. 524–535, 2021.
 - [10] H. Hassan and S. Harmand, “An experimental and numerical study on the effects of the flat heat pipe wick structure on its thermal performance,” *Heat Transfer Engineering*, vol. 36, no. 3, pp. 278–289, 2015.
 - [11] S. A. Al-Mabsali, H. N. Chaudhry, and M. S. Gul, “Numerical investigation on heat pipe spanwise spacing to determine optimum configuration for passive cooling of photovoltaic panels,” *Energies*, vol. 12, no. 24, p. 4635, 2019.
 - [12] S. Arabnejad, R. Rasoulian, M. B. Shafii, and Y. Saboohi, “Numerical investigation of the performance of a U-shaped pulsating heat pipe,” *Heat Transfer Engineering*, vol. 31, no. 14, pp. 1155–1164, 2010.
 - [13] G. Kumaresan, P. Vijayakumar, M. Ravikumar, R. Kamatchi, and P. Selvakumar, “Experimental study on effect of wick structures on thermal performance enhancement of cylindrical heat pipes,” *Journal of Thermal Analysis and Calorimetry*, vol. 136, no. 1, pp. 389–400, 2019.
 - [14] S. Miao, J. Sui, Y. Zhang, F. Yao, and X. Liu, “Experimental study on thermal performance of a bent copper-water heat pipe,” *International Journal of Aerospace Engineering*, vol. 2020, Article ID 8632152, 10 pages, 2020.
 - [15] D. D. Odhekar and D. K. Harris, “Experimental investigation of bendable heat pipes using sintered copper felt wick,” in *Thermal and Thermomechanical Proceedings 10th Intersociety Conference on Phenomena in Electronics Systems, 2006. ITherm 2006*, pp. 570–577, San Diego, CA, USA, 2006.
 - [16] J. Zhang, L. X. Lian, Y. Liu, and R. Q. Wang, “The heat transfer capability prediction of heat pipes based on capillary rise test of wicks,” *International Journal of Heat and Mass Transfer*, vol. 164, article 120536, 2021.
 - [17] H. Li, X. Fang, G. Li, G. Zhou, and Y. Tang, “Investigation on fabrication and capillary performance of multi-scale composite porous wick made by alloying-dealloying method,” *International Journal of Heat and Mass Transfer*, vol. 127, pp. 145–153, 2018.
 - [18] D. Jafari, W. W. Wits, and B. J. Geurts, “Phase change heat transfer characteristics of an additively manufactured wick for heat pipe applications,” *Applied Thermal Engineering*, vol. 168, p. 114890, 2020.
 - [19] M. Vijayakumar, P. Navaneethakrishnan, and G. Kumaresan, “Thermal characteristics studies on sintered wick heat pipe using CuO and Al₂O₃ nanofluids,” *Experimental Thermal and Fluid Science*, vol. 79, pp. 25–35, 2016.
 - [20] A. Brautsch and P. A. Kew, “Examination and visualisation of heat transfer processes during evaporation in capillary porous structures,” *Applied Thermal Engineering*, vol. 22, no. 7, pp. 815–824, 2002.
 - [21] I. L. Ngo and C. Byon, “Permeability of microporous wicks with geometric inverse to sintered particles,” *International Journal of Heat and Mass Transfer*, vol. 92, pp. 298–302, 2016.
 - [22] S. Zhang, C. Chen, G. Chen, Y. Sun, Y. Tang, and Z. Wang, “Capillary performance characterization of porous sintered stainless steel powder wicks for stainless steel heat pipes,” *International Communications in Heat and Mass Transfer*, vol. 116, article 104702, 2020.
 - [23] R. K. Bumataria, N. K. Chavda, and H. Panchal, “Current research aspects in mono and hybrid nanofluid based heat pipe technologies,” *Heliyon*, vol. 5, no. 5, article e01627, 2019.
 - [24] R. K. Bumataria, N. K. Chavda, and A. H. Nalbandh, “Performance evaluation of the cylindrical shaped heat pipe utilizing water-based CuO and ZnO hybrid nanofluids,” *Energy Sources, Part A: Recovery, Utilization, and Environmental Effects*, pp. 1–16, 2020.
 - [25] R. Bumataria and N. Chavda, “Heat load and orientation impacts in cylindrical heat pipes using copper oxide, aluminium oxide, and zinc oxide nanofluids,” *International Journal of Ambient Energy*, pp. 1–11, 2021.
 - [26] P. M. J. Stalin, T. V. Arjunan, M. Almeshaal, P. Murugesan, B. Prabu, and P. M. Kumar, “Utilization of zinc-ferrite/water hybrid nanofluids on thermal performance of a flat plate solar collector—a thermal modeling approach,” *Environmental Science and Pollution Research*, pp. 1–14, 2022.
 - [27] R. Sharma, P. Chauhan, A. K. Sharma et al., “Characterization of ZnO/Nanofluid for Improving Heat Transfer in Thermal Systems,” *Materials Today: Proceedings*, vol. 62, pp. 1904–1908, 2022.
 - [28] J. P. Holman, *Experimental Methods for Engineers*, McGraw Hill, 2001.
 - [29] G. Kumaresan, S. Venkatachalapathy, L. G. Asirvatham, and S. Wongwises, “Comparative study on heat transfer characteristics of sintered and mesh wick heat pipes using CuO nanofluids,” *International Communications in Heat and Mass Transfer*, vol. 57, pp. 208–215, 2014.
 - [30] G. Kumaresan, S. Venkatachalapathy, and L. G. Asirvatham, “Experimental investigation on enhancement in thermal characteristics of sintered wick heat pipe using CuO nanofluids,” *International Journal of Heat and Mass Transfer*, vol. 72, pp. 507–516, 2014.
 - [31] Z. Said, P. S. Shekrahmana, A. A. Hachicha, and S. Issa, “Performance characterization of a solar-powered shell and tube heat exchanger utilizing MWCNTs/water-based nanofluids: an experimental, numerical, and artificial intelligence approach,” *Applied Thermal Engineering*, vol. 212, no. 25, 2022.
 - [32] P. M. J. Stalin, T. V. Arjunan, M. M. Matheswaran, P. M. Kumar, and N. Sadanandam, “Investigations on thermal properties of CeO₂/water nanofluids for heat transfer applications,” *Materials Today: Proceedings*, vol. 47, pp. 6815–6820, 2021.